Iron fertilisation and century-scale effects of open ocean dissolution of olivine in a simulated CO_2 removal experiment

Environmental Research Letters

LETTER

Iron fertilisation and century-scale effects of open ocean dissolution of olivine in a simulated CO_2 removal experiment

Judith Hauck, Peter Köhler, Dieter Wolf-Gladrow and Christoph Völker

Alfred-Wegener-Institut, Helmholtz-Zentrum für Polar- und Meeresforschung, Am Handelshafen 12, D-27570 Bremerhaven, Germany

E-mail: judith.hauck@awi.de

Keywords: geoengineering, carbon dioxide removal, enhanced weathering, biological carbon pump, iron fertilisation, ocean alkalinisation

Supplementary material for this article is available online

OPEN ACCESS

RECEIVED
27 October 2015

REVISED
13 January 2016

ACCEPTED FOR PUBLICATION
14 January 2016

PUBLISHED
9 February 2016

Abstract

Carbon dioxide removal (CDR) approaches are efforts to reduce the atmospheric CO_2 concentration. Here we use a marine carbon cycle model to investigate the effects of one CDR technique: the open ocean dissolution of the iron-containing mineral olivine. We analyse the maximum CDR potential of an annual dissolution of 3 Pg olivine during the 21st century and focus on the role of the micro-nutrient iron for the biological carbon pump. Distributing the products of olivine dissolution (bicarbonate, silicic acid, iron) uniformly in the global surface ocean has a maximum CDR potential of 0.57 gC/g-olivine mainly due to the alkalinisation of the ocean, with a significant contribution from the fertilisation of phytoplankton with silicic acid and iron. The part of the CDR caused by ocean fertilisation is not permanent, while the CO_2 sequestered by alkalinisation would be stored in the ocean as long as alkalinity is not removed from the system. For high CO_2 emission scenarios the CDR potential due to the alkalinity input becomes more efficient over time with increasing ocean acidification. The alkalinity-induced CDR potential scales linearly with the amount of olivine, while the iron-induced CDR saturates at 113 PgC per century (on average $\sim$1.1 PgC yr^{-1}) for an iron input rate of 2.3 Tg Fe yr^{-1} (1% of the iron contained in 3 Pg olivine). The additional iron-related CO_2 uptake occurs in the Southern Ocean and in the iron-limited regions of the Pacific. Effects of this approach on surface ocean pH are small ($<$0.01).

1. Introduction

Humans perturb the CO_2 concentration in the atmosphere by burning of fossil fuels and by land use change. CO_2 is a greenhouse gas and its accumulation in the atmosphere leads to a warming of the Earth system, and to changes in all parts of the climate system, e.g. the hydrological cycle. About a quarter of the annual CO_2 emissions is taken up by the ocean (Le Quéré *et al* 2015), leading to acidification with potentially detrimental effects for ocean ecosystems and their services to humans (Pörtner *et al* 2014).

Most IPCC emission scenarios project a warming of more than 2 °C compared to pre-industrial levels by the end of the 21st century (IPCC 2013, Rogelj *et al* 2015), hence a large effort is needed to keep the temperature rise below the agreed-upon threshold of 2 °C (UNFCCC 2009). To stay below this threshold, zero and net negative emissions might be necessary from 2060 onwards (Rogelj *et al* 2015). Owing to this necessity, besides taking action to reduce carbon emissions, two types of geoengineering methods have been proposed to counteract global warming. Albedo modification (or 'solar radiation management') is considered a 'quick-fix' that could counteract the warming on the time-scale of years at relatively low cost (Kravitz *et al* 2011, National Research Council 2015). However, its side-effects are poorly understood and applying albedo modification at global scale would lead to regional impacts, such as further changes in precipitation patterns (Kravitz *et al* 2013, National Research Council 2015). Albedo modification might cool the planet. As side effects of these approaches the carbon cycle might also be influenced, potentially leading to large variations in atmospheric CO_2, e.g. a cooler ocean might store more CO_2

(Oschlies *et al* 2010b, Keller *et al* 2014), temperature and precipitation changes on land might impact the terrestrial carbon cycle (Oschlies *et al* 2010b, Kravitz *et al* 2013, Glienke *et al* 2015). A termination of the albedo modification measure would lead to a large and sudden temperature rise (Jones *et al* 2013). The second type of geoengineering approaches are carbon dioxide removal (CDR) methods which directly address the cause of climate change. As atmospheric CO_2 would be lowered by CDR methods, carbon from natural ocean and land sinks would degas until a new equilibrium is established. Due to this rebound effect, not only the accumulated anthropogenic CO_2 in the atmosphere, but about twice this amount of CO_2 has to be removed from the atmosphere for any intended atmospheric CO_2 reduction (e.g. 42 Gt of carbon needs to be removed from the system to reduce atmospheric CO_2 by 10 ppmv or 21 GtC) (Cao and Caldeira 2010a, Matthews 2010).

One such CDR method is enhanced weathering (or dissolution) of silicate rocks (Hartmann *et al* 2013). On geological time-scales, natural weathering will be the ultimate sink for anthropogenic CO_2 emissions (Archer 2005). An abundant magnesium silicate which dissolves in contact with CO_2 and water is olivine ($(Mg,Fe)_2SiO_4$, Schuiling and Krijgsman 2006):

$$(Mg, Fe)_2SiO_4 + 4CO_2 + 4H_2O \rightarrow 2(Mg, Fe)^{2+} + 4HCO_3^- + H_4SiO_4. \quad (1)$$

The reaction products, bicarbonate, silicic acid and Mg and Fe are transported to the oceans following the dissolution on land. Carbon is sequestered in the ocean in the form of bicarbonate and the increase of alkalinity leads to an increase of pH and further enhances the CO_2 uptake capability of the ocean (Köhler *et al* 2010). Direct open ocean dissolution of olivine additionally stimulates biological production and CO_2 sequestration due to the fertilising effect of the additional silicate (Köhler *et al* 2013). Olivine also contains iron which is a limiting micronutrient for phytoplankton production in extended ocean regions, such as the Southern Ocean (De Baar *et al* 1995, Smetacek *et al* 2012), the subpolar North Pacific (Martin and Fitzwater 1988), and large parts of the South Pacific (Behrenfeld *et al* 2009). However, the impact of iron fertilisation (a proposed CDR method of its own, Zeebe and Archer 2005, Aumont and Bopp 2006, Smetacek *et al* 2012) during open ocean dissolution of olivine was not quantified in previous studies.

The fraction of iron that goes into solution when lithogenic material such as dust is deposited in seawater varies between 0.01% and 80%, depending on a variety of factors that are not completely understood, such as mineralogy, chemical processing during atmospheric transport, wet versus dry deposition, and the concentration of organic iron-binding ligands in seawater (Baker and Croot 2010). Compared to other iron-containing minerals such as iron-oxyhydroxides, olivine is expected to dissolve more readily, so that we could expect the fraction of iron dissolved to be on the higher side. However, due to the low solubility of iron in seawater (Liu and Millero 2002) some of the iron from olivine is likely to quickly form iron-oxyhydroxide colloids and be scavenged onto available particles (Honeyman and Santschi 1989, Rose and Waite 2007). The degree to which this will happen depends also on whether the concentration of iron after dissolution of olivine exceeds that of organic iron-binding ligands present in seawater (Fishwick *et al* 2014), which is typically on the order of one to a few nmol l^{-1} in open oceans. The fraction of iron from olivine that ultimately becomes bioavailable is therefore hard to estimate at this point without further experimentation and thus we will explore a range of values (sensitivity analysis).

In this study, we aim to quantify the potential impact of iron fertilisation on the efficiency of olivine dissolution as a CDR method on a centennial time-scale, as well as its effects on primary production, carbon export and the abundance of phytoplankton functional types. We particularly strive to assess the sensitivity of CDR efficiency to the fraction of iron in olivine that becomes dissolved and stays long enough in solution to become bioavailable (which for brevity we call 'availability' in the following).

2. Model and numerical experiments

We use the marine regulated ecosystem and biogeochemistry model REcoM2 (Hauck *et al* 2013) coupled to the Massachusetts Institute of Technology general circulation model (MITgcm, Marshall *et al* 1997, MITgcm Group 2015). This model was also used in our previous study on the open ocean dissolution of olivine (Köhler *et al* 2013).

The model is configured globally without the Arctic Ocean. The resolution is 2° in longitude and 1/3 to 2° in latitude with higher resolution around the equator and in the Southern Hemisphere where the latitudinal resolution is scaled by the cosine of the latitude. The model has 30 depth levels and the vertical resolution decreases from 10 m at the surface to 500 m in the deep ocean.

The ecosystem model REcoM2 (Hauck *et al* 2013) carries 21 tracers, including the dissolved inorganic nutrients nitrate, silicic acid and iron. The intracellular pools of carbon, chlorophyll, nitrogen, silicon and $CaCO_3$ for the two phytoplankton groups, diatoms and nanophytoplankton, are explicitly modelled and allow for dynamic intracellular stoichiometry, following Geider *et al* (1998). Detrital carbon, nitrogen, silicon and calcium carbonate are actively advected until degradation or remineralisation occurs.

The model has undergone some development since the study of Hauck *et al* (2013). Besides updating the MITgcm to the latest version (checkpoint 65n), the

Table 1. Model simulations. In all olivine dissolution experiments, 3 Pg of olivine are dissolved per year for the years 2000–2099. In the simulations with termination effect, olivine addition is stopped after 10 years.

Short name	Description
CTRL	Control simulation, no olivine dissolution
ALK	Only alkalinity
SI+ALK	Silicic acid and alkalinity
FE_1	Only iron effect, 1% Fe-availability
SI+ALK+FE_0.1	Silicic acid, alkalinity and iron, 0.1% Fe-availability
SI+ALK+FE_1	Silicic acid, alkalinity and iron, 1% Fe-availability
SI+ALK+FE_10	Silicic acid, alkalinity and iron, 10% Fe-availability
SI+ALK+FE_100	Silicic acid, alkalinity and iron, 100% Fe-availability
ALK_T	Only alkalinity, with termination effect
SI+ALK+FE_1T	Silicic acid, alkalinity and iron, 1% Fe-availability, with termination effect

intracellular iron pool was made dependent on nitrogen (fixed Fe:N instead of Fe:C) as iron is physiologically rather linked to enzyme formation, especially the photosynthetic electron transport chain (Raven 1988, Behrenfeld and Milligan 2013) than to overall biomass that also includes carbohydrates and fatty acids. Furthermore, we included sedimentary sources of iron and we increased the ligand stability constant to 200 $m^3\ \mu mol^{-1}$ and the iron solubility from 1% to 2%. The maximum chlorophyll to nitrogen ratio was set to 3.78 mg Chl $(mmol\ N)^{-1}$ and the diatom chlorophyll degradation rate to 0.1 d^{-1}.

The model is spun-up from 1900 to 1999 and we start the addition of olivine in the model year 2000 and run the model for 100 years (2000–2099). The model is forced with the normal year atmospheric forcing fields from the coordinated ocean research experiments (Large and Yeager 2009) during the spin-up and experimental period. Atmospheric CO_2 is prescribed by a spline-fit to ice-core data (Enting *et al* 1994) until 1957, by the annually averaged Mauna Loa CO_2 data after 1958 (Keeling *et al* 2009), and follows RCP8.5 from 2010 until 2099 reaching more than 900 ppm at the end of the century (Meinshausen *et al* 2011, van Vuuren *et al* 2011). Prescribing atmospheric CO_2 is a simplification that underestimates sea-to-air back fluxes. Together with the omission of resulting variations in land carbon pools, this might lead to an overestimation of the CDR potential of the analysed approach that is dependent on the emission scenario (Oschlies 2009). As our model set-up uses climatological atmospheric forcing, we consider the effect of increasing atmospheric CO_2 over that time period but no effects of climate change, such as warming and circulation changes. This setup has the advantage that the changes in biological production caused by olivine dissolution are rather independent from the chosen emission scenario. The disadvantage of this approach is that synergies between olivine dissolution and warming/circulation effects are omitted, however, we consider them to play only a secondary role.

We perform one control (CTRL, see table 1) simulation without addition of olivine, in all other simulations we add dissolved olivine to the surface ocean. Since this study is a follow-up of our previous analysis (Köhler *et al* 2013) we use the same dissolution scenario of 3 Pg of olivine per year. This choice is also supported by our previous finding that the alkalinity and silicic acid induced CDR potential scale linearly with the amount of dissolved olivine and by the fact that present day coal production (the largest global mining activity) was ~8 Pg in year 2013 (International Energy Agency 2014), making a significantly larger annual olivine production over a short time rather unlikely. The olivine is assumed to dissolve immediately and completely and is spread uniformally throughout the year and over the entire surface ocean (standard scenario in Köhler *et al* 2013). In doing so, we aim for estimating the potential or upper limit of the approach. The importance of grain size, mixed layer depth, and sea surface temperature on the dissolution rates of olivine have already been discussed together with related energy costs in Köhler *et al* (2013) and is not repeated here. Assuming immediate and complete dissolution of olivine is thus an effort to estimate the maximum effects or the overall potential of the approach. Besides the control run, we perform model simulations in which we consider only the effects of alkalinity (ALK), and the joint effects of silicic acid and alkalinity but no iron (SI+ALK) from olivine dissolution. These two simulations are described in detail in Köhler *et al* (2013), but are repeated here to monitor the system response over 100 years in the modified model set-up.

The sensitivity of carbon removal efficiency by olivine dissolution to iron solubility, scavenging and colloid formation is assessed by four model simulations in which silicic acid, alkalinity and iron are simultaneously released from olivine with iron availabilities of 0.1%, 1%, 10%, and 100% (SI+ALK+FE_X, where X describes the availability of iron). Olivine is assumed to have a molar weight of 147 g mol^{-1} and a Mg:Fe molar ratio of 9:1 typically found in nature (De Hoog *et al* 2010). Specifically, following equation (1), we increase alkalinity by 4 mol, silicate by 1 mol and iron by 0.2 mol per mol of olivine dissolved. The total amount of added iron is 0.23 Tg yr^{-1} in the 0.1% availability case. This is approximately the same

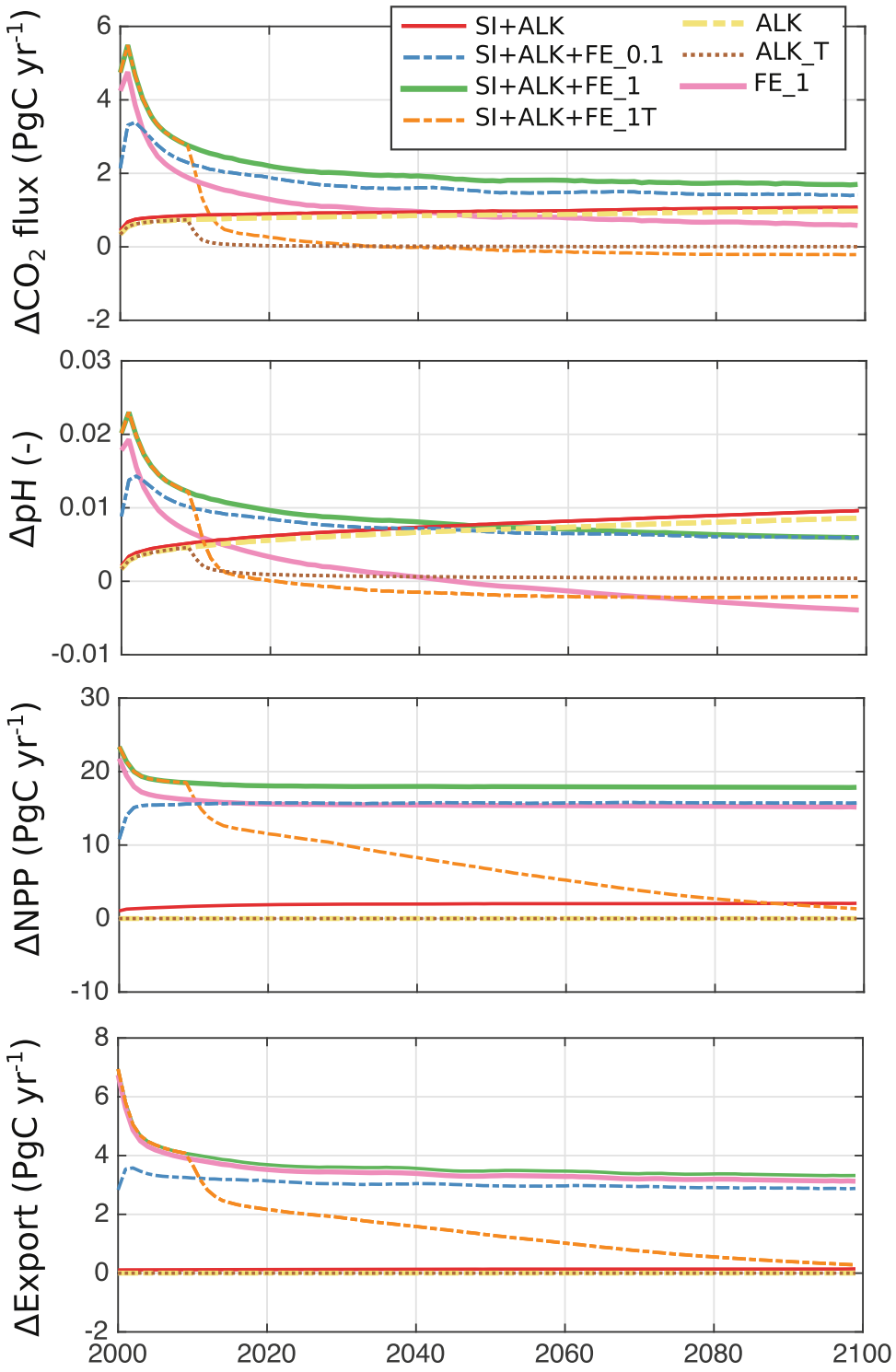

Figure 1. Timeseries of CO_2 flux, pH, NPP and export production in different olivine dissolution scenarios relative to the control run. See table 1 for the list of simulations. Note that SI+ALK+FE_10 and SI+ALK+FE_100 are not shown for reasons of readability as they overlay the SI+ALK+FE_1 line.

number as the bioavailable iron input by dust (Mahowald *et al* 2005).

We also conduct two experiments to explore the termination effect of olivine input. In the termination experiments, we dissolve olivine for ten years and continue the model run for another 90 years without olivine dissolution. The termination experiments are conducted for the case where only alkalinity is considered (ALK_T) and for the case of joint consideration of alkalinity, silicic acid and iron with an Fe-availability of 1% (SI+ALK+FE_1T).

Furthermore, we conduct an additional simulation for the 1% availability case, where we only consider the addition of iron (FE_1), without increasing

Table 2. Marine CO_2 uptake (FCO_2), pH, export production, total, nanophytoplankton and diatom net primary production (NPP, NPPS and NPPD, respectively) in the CTRL, in the SI+ALK simulation and in the simulations with iron availability varying between 0.1% and 10%. Numbers are means over the last ten years (2090–2099) of the simulation and in all experiments 3 Pg of olivine per year are dissolved. All units are PgC yr^{-1}, except pH which is unitless. T stands for the run with the termination effect.

	CTRL	ALK	SI+ALK	SI+ALK+FE			
				0.1%	1%	1% T	10%
Global							
FCO_2	6.0	7.0	7.1	7.5	7.7	5.8	7.8
pH	7.746	7.754	7.755	7.752	7.752	7.744	7.752
Export	10.2	10.2	10.4	13.1	13.5	10.6	13.6
NPP	40.4	40.4	42.5	56.2	58.3	42.1	58.5
NPPS	22.4	22.4	19.2	29.2	29.1	23.4	29.0
NPPD	18.1	18.1	23.3	27.0	29.2	18.6	29.4
South of 40°S							
FCO_2	2.5	2.7	2.8	3.1	3.4	2.5	3.4
pH	7.732	7.737	7.738	7.736	7.736	7.730	7.736
Export	2.9	2.9	2.9	3.8	4.2	3.0	4.2
NPP	7.2	7.2	7.4	9.8	11.8	7.4	11.9
NPPS	1.6	1.6	1.3	1.9	1.9	1.8	1.9
NPPD	5.5	5.5	6.2	7.9	9.9	5.6	10.0

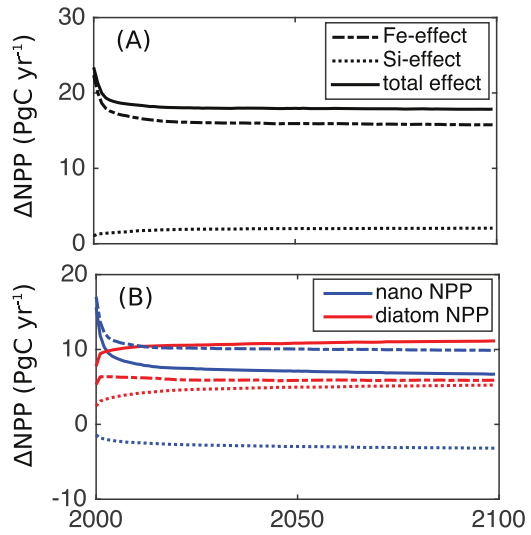

Figure 2. Effect of olivine dissolution on NPP: time-series of (A) total, (B) diatom (red) and nanophytoplankton (blue) NPP in the SI+ALK+FE_1 simulation relative to the CTRL simulation (full line) and the contributions of iron (dashed line) and silicic acid (dotted line) fertilisation effects.

silicic acid and alkalinity, to investigate whether there are synergistic effects by simultaneously adding iron and silicic acid. Table 1 contains an overview of the performed simulation scenarios.

3. Results and discussion

Model results without olivine dissolution were published elsewhere (Hauck *et al* 2013, Köhler *et al* 2013, Hauck and Völker 2015). The model has changed slightly, hence we show global maps of mean export production, diatom, nanophytoplankton and total net primary production (NPP), pH and CO_2 flux in the first ten years of the CTRL simulation and the temporal evolution of the surface iron concentration in the supplement (figures S2 and S3). The results of the mean state do not differ significantly from the previous version and we therefore refer the reader to the main text and supplement of Hauck *et al* (2013) and Köhler *et al* (2013) for further information. In the following we restrict our analysis to anomalies in the carbon cycle obtained from the assumed olivine dissolution.

3.1. Simulation of iron fertilisation within the concept of open ocean olivine dissolution

The additional consideration of iron fertilisation amplifies the alkalinity- and silicate-based CDR of olivine dissolution, leading to further increase of the potential oceanic CO_2 uptake, NPP and export production (figure 1, table 2).

In the last decade of the simulation scenarios, the total effect of olivine dissolution with the 0.1% (1%) iron availability scenario leads to an additional CO_2 uptake of 1.4 PgC yr^{-1} (1.6 PgC yr^{-1}) or a rise by +24% (+28%) compared to the CTRL. The relative contributions of alkalinity, silicic acid and iron in the 0.1% (1%) scenario amount to 69% (57%), 7% (6%) and 24% (37%), respectively. The effect of iron fertilisation saturates already at an availability of 1% with a maximum in Fe-driven CO_2 uptake of 0.6 PgC yr^{-1} or 0.2 PgC per Pg olivine in the last ten years of the simulation (figure 1(a)).

The annual mean pH is 0.006 units higher than in CTRL at the end of the olivine dissolution simulation with 0.1% Fe-availability. The effects of alkalinity (0.009) and silicic acid (0.001) lead to a larger pH restoration, however, the iron effect leads to an increase of pH initially, but to a decrease of pH after

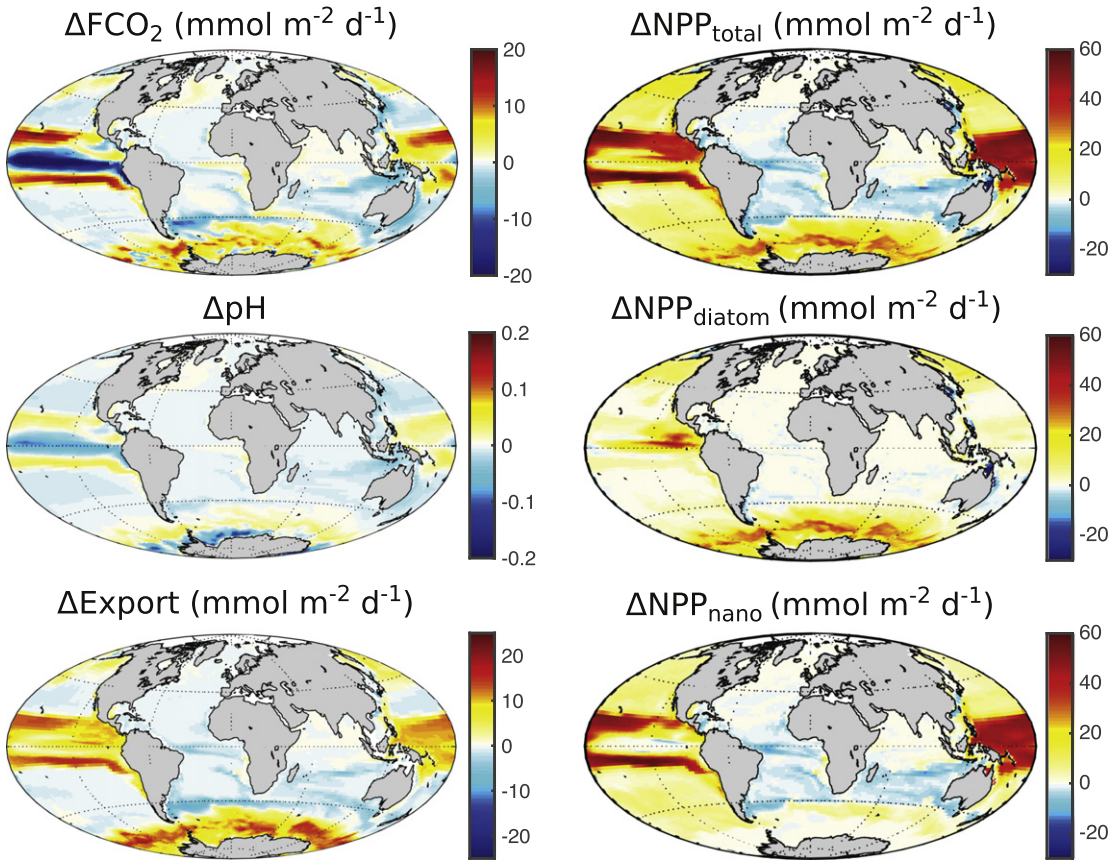

Figure 3. Effects of iron during olivine dissolution on CO_2 flux (FCO_2, positive: into ocean, mmol m^{-2} d^{-1}), pH, export production (mmol m^{-2} d^{-1}), total, diatom and nanophytoplankton NPP (all mmol m^{-2} d^{-1}) in the last ten years of the simulation with 3 Pg olivine dissolution and 1% iron availability (SI+ALK+FE_1), relative to the SI+ALK simulation.

approximately 50 years when the transport of remineralised carbon reaches the surface and outweighs the current carbon draw-down by iron fertilisation (figure 1(b)). A termination of the open ocean dissolution of olivine results in a lower pH relative to the unperturbed CTRL state only 10 years after the termination. The pH increase due to olivine dissolution is small compared to the pH decrease driven by anthropogenic carbon uptake from about 8.1 to < 7.8 in our simulations over the 21st century.

Diatom NPP increases by 9.0 PgC yr^{-1} or 50% after 100 years in the low (0.1%) Fe-availability scenario. Here, silicic acid contributes 58% and Fe-fertilisation 42% to the total rise in diatom NPP. Diatom primary production can be increased by a maximum of 11 PgC yr^{-1} by olivine addition when an Fe-availability $\geqslant$1% is assumed (figure 2(b)). Nanophytoplankton NPP simultaneously increases by 6.8 PgC yr^{-1} or 30% and saturates already at 0.1% iron availability (table 2, figure 2(b)). In total, the enhancement of NPP through the input of silicic acid and iron as biproducts of the olivine dissolution amount to +39% or +15.7 PgC yr^{-1} in the 0.1% availability scenario and to +45% or +18.0 PgC yr^{-1} in the 1% availability scenario with a relative contribution of ~90% from iron (figures 1(c), 2(a)).

While silicic acid favours a shift towards diatoms (see table 2 and Köhler *et al* 2013), iron stimulates NPP of both diatoms and nanophytoplankton (figures 2 and 3 and Aumont and Bopp 2006).

In the last ten years of the simulation, diatom NPP changes based on Fe fertilisation are strongest in the Southern Ocean and in the equatorial and North Pacific, and close to zero in the remaining ocean basins. Nanophytoplankton NPP thrives outside the areas where diatoms profit: in a band to the North of the Southern Ocean and in the whole Pacific except the equatorial East Pacific (figure 3). Nanophytoplankton NPP is reduced in the Atlantic Ocean and in the subtropical Indian Ocean where iron is not the most limiting nutrient in the CTRL simulation (figure 4). The largest increase in CO_2 uptake is in the Southern Ocean and in a band north and south of the eastern equatorial upwelling area in the Pacific with minor contributions from the north Pacific and north Atlantic. In the eastern equatorial upwelling area itself a strong decrease of CO_2 uptake is detected (figure 3).

Globally, the export production of particulate organic matter at 100 m water depth increases by 2.9 PgC yr^{-1} (+28%) at the end of the 100 years simulation (0.1% Fe-availability) with a dominance of the iron fertilisation effect (+2.7 PgC yr^{-1}) over that of silicic acid fertilisation (0.2 PgC yr^{-1}). At maximum

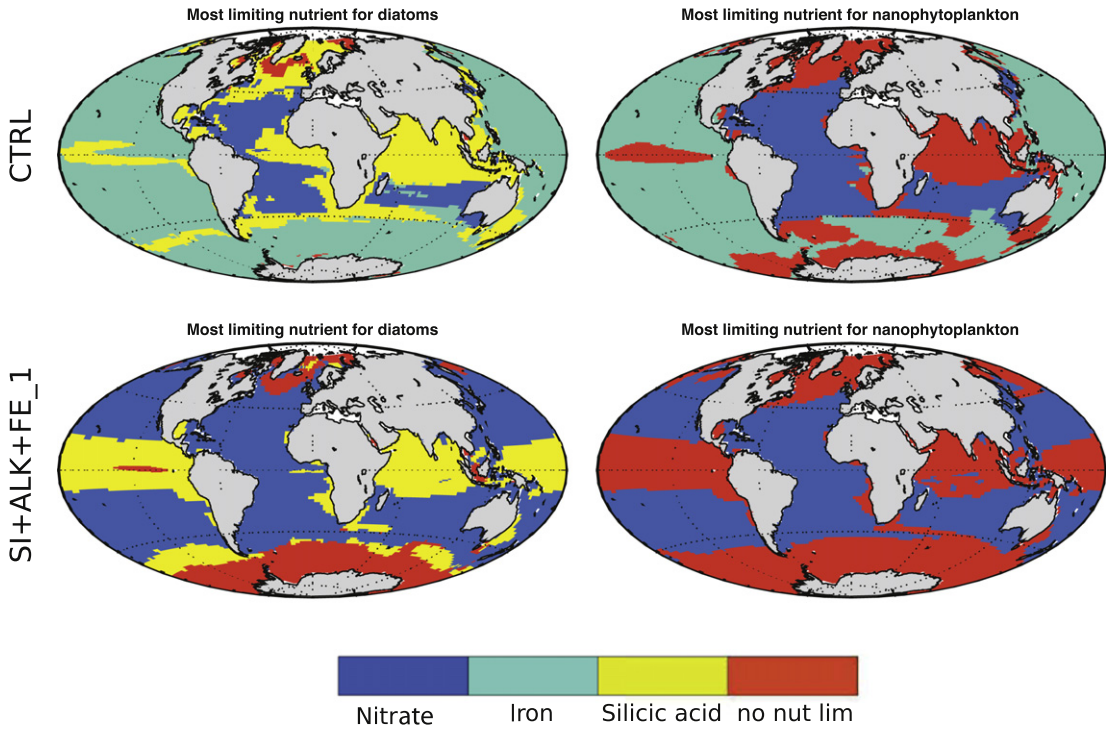

Figure 4. The most limiting nutrient for diatom (left) and nanophytoplankton (right) growth in the CTRL (top) and SI+ALK+FE_1 (bottom) simulations, average over 2090–2099. When no limitation factor is below 0.7, we assume that nutrients are not limiting, but rather light or temperature.

an additional export of 3.3 PgC yr^{-1} can be obtained by olivine dissolution for an availability of iron of 1% or more (table 2, figure 1(d)).

The largest effects of iron fertilisation by olivine dissolution occur within the first ten years of the simulations (figure 1). When terminating the continuous dissolution of olivine, the dominant part of the benefit of the larger oceanic CO_2 uptake is lost within a few years and a state close to the control simulation without olivine addition is reached within approximately one decade (figure 1). Terminating open ocean dissolution of olivine dissolution leads to a lower pH relative to the CTRL simulation ten years after the termination (−0.002 in the last decade of the simulation) and to a loss of oceanic CO_2 to the atmosphere relative to CTRL 25 years after the termination (−0.2 PgC yr^{-1} in the last decade of the simulation). However, the cumulative sum of CO_2 uptake is at every time higher in the SI+ALK+FE_1T simulation than in the CTRL, indicating that the release of the remineralised carbon to the atmosphere is rather slow. Net primary and export production show a slower recovery to pre-olivine conditions and are still enhanced relative to the CTRL simulation at the end of the simulations.

Nearly all of the iron-effect on production, pH and CO_2 flux occur in the Southern Ocean and in the Pacific (figure 3) where iron is the most-limiting nutrient in our CTRL simulation (figure 4). Despite the relatively short spin-up and a decreasing trend in global surface iron concentration (−6% over 100 years) that is caused by regions where iron is not a limiting nutrient (Atlantic and Indian Oceans), the surface iron concentrations in the Southern Ocean and in the Pacific vary little over time in the CTRL simulation and show no clear linear trend (figure S3). In addition, the surface iron perturbation by olivine dissolution is much larger than any temporal variability in these regions (figure S3). We can thus assume, that the response to iron addition does not change over time due to model drift. In the Pacific Ocean, models differ in the degree and extent of iron limited regions (Laufkötter *et al* 2015) and the response of primary production to iron addition will be model dependent. Traditionally, it is assumed that iron is the most limiting nutrient in high-nutrient-low-chlorophyll (HNLC) regions. Recent evidence, however, suggests that iron can also be a limiting factor in non-HNLC regions on a seasonal scale (e.g., Nielsdóttir *et al* 2009). Behrenfeld *et al* (2009) report strong evidence for iron (co-)limitation in large areas of the south Pacific Ocean.

The consumption of additional macronutrients along with the micronutrient iron in the Southern Ocean leads to nutrient depletion in Antarctic surface waters that get subducted to form northwards moving mode waters. The effects of this nutrient depletion become apparent only in the Atlantic and Indian Ocean in our model where NPP is reduced north of 40°S (figure 3). This is in line with the current understanding that the inefficiency of the biological carbon pump in the Southern Ocean due to the iron deficiency fuels present-day biological production in low

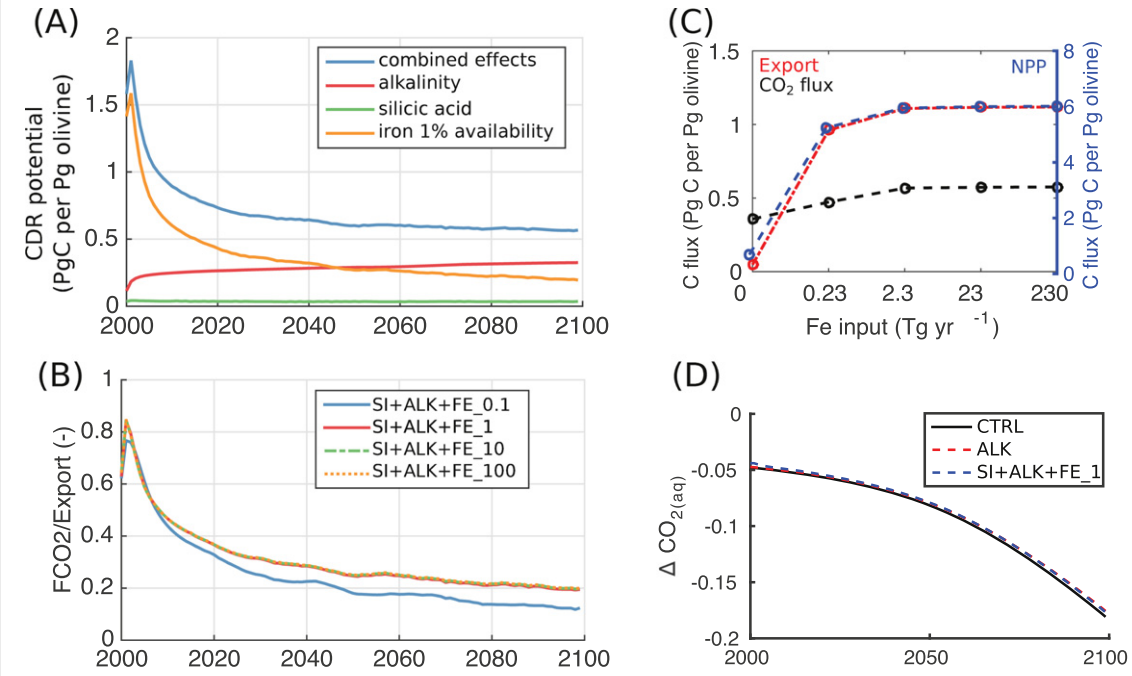

Figure 5. (A) The temporal evolution of carbon sequestration potential of olivine assuming a 1% Fe-availability and the contributions of silicic acid, alkalinity and iron (1% availability). The alkalinity effect increases over time due to the higher sensitivity of dissolved CO_2 to alkalinity perturbation in a high CO_2 ocean, whereas the iron effect decreases over time due to the remineralisation of organic carbon and its transport to the surface. See text. (B) Ratio of ΔCO_2 uptake to Δ export in full olivine dissolution scenarios (SI+ALK +FE) with varying Fe-availability relative to the SI+ALK simulation. Results for 1%, 10% and 100% Fe-availability overlay each other. (C) ΔCO_2 flux (black, left axis), Δexport production (red, left axis) and ΔNPP (blue, right axis) for 3 Pg olivine dissolved, dependent on the total amount of iron that is released. Average over last ten years of model run (2090–2099). Note that Δexport at 0 Fe input is 0.07 PgC per Pg olivine (see SI+ALK in table 2). (D) The sensitivity of $CO_{2\,(aq)}$ to an alkalinity addition of 1 mmol m^{-3} in the CTRL, ALK and SI+ALK+FE_1 simulations, that hardly differ.

latitudes (Sarmiento *et al* 2004). An enhanced efficiency of the biological carbon pump in the Southern Ocean therefore reduces NPP in lower latitude upwelling regions on multi-decadal to centennial timescales (Rodgers *et al* 2003).

We also tested for synergistic effects of silicic acid and iron addition by comparing the iron effect in an iron-only scenario (FE_1) to the joint addition of iron with alkalinity and silicic acid (SI+ALK+FE_1). Synergistic effects favour diatom NPP, which is affected most strongly at the start of the simulation ($+1.5$ PgC yr^{-1}), and decreases over time to about $+0.7$ PgC yr^{-1} in model year 2099 (figure S1). The simultaneous addition of silicic acid and iron has a negative effect on nanophytoplankton NPP (-1 PgC yr^{-1} in year 2000, -0.1 PgC yr^{-1} in year 2099). Synergistic effects on total NPP, export production and CO_2 flux are about 0.6, 0.05 and 0.03 PgC yr^{-1} in year 2099, respectively, and are small in comparison to the iron effect itself.

All carbon fluxes saturate at an available iron input of 2.3 Tg Fe yr^{-1} (or a one-time per year increase of 1.1 nmol Fe L^{-1} in the upper 100 m; 1% Fe-availability scenario) in our set of simulations (figure 5(c)). The potential of carbon sequestration by olivine dissolution increases from 0.36 PgC per Pg olivine (SI +ALK) after 100 years to 0.57 PgC yr^{-1} per Pg olivine when considering the iron fertilisation effect with an availability of 1%.

The carbon uptake potential after a century from alkalinity and silicic acid effects is larger than the 0.28 PgC per Pg olivine that was found after 10 years in Köhler *et al* (2013). This difference can be explained by the steady increase of the CO_2 flux response to alkalinisation (32% increase to 0.33 PgC per Pg olivine from 2010 to 2099, figure 5(a)). We explain this temporal evolution of alkalinity-driven CO_2 uptake by the increased sensitivity of $CO_{2\,(aq)}$ and consequently CO_2 flux to alkalinity and carbon perturbations in a high-CO_2 ocean (Egleston *et al* 2010, Hauck and Völker 2015). We illustrate the four-fold increase of the sensitivity of $CO_{2(aq)}$ to alkalinity input over 100 years in figure 5(d). This sensitivity is calculated as

$$\Delta[CO_{2(aq)}] = \frac{\Delta Alk}{\gamma_{Alk}}[CO_{2(aq)}]. \qquad (2)$$

with $\Delta Alk = 1$ mmol m^{-3} and with output from CO2SYS which is run with model fields of surface DIC, alkalinity, temperature, salinity, dissolved silicic acid and phosphate (converted from the modelled nitrate fields by the Redfield ratio). γ_{Alk} is defined according to Egleston *et al* (2010):

$$\gamma_{Alk} = \left(\frac{\partial \ln[CO_{2\,(aq)}]}{\partial Alk}\right)^{-1}. \qquad (3)$$

This rise in the CO_2 uptake of the ocean due to the alkalinity input depends on the assumed changes in the anthropogenic emissions and would be smaller in other RCP scenarios with lower atmospheric CO_2 concentrations.

The alkalinity effect on CO_2 uptake due to olivine dissolution can be considered permanent in the sense that even after a termination, CO_2 uptake will always be larger or equal to CTRL and the sequestered carbon will not be released to the atmosphere as long as alkalinity is not removed from the ocean. However, the iron effect of olivine addition is temporary, i.e. terminating an olivine dissolution experiment that releases significant amounts of iron would lead to a reduced CO_2 uptake capacity after the termination, i.e. in our model the CO_2 uptake is reduced relative to the CTRL simulation three decades after the termination (figure 1).

3.2. Discussing iron fertilisation

The CDR potential of iron fertilisation decreases over time from 1.6 to 0.2 PgC per Pg olivine (or from 4.8 to 0.6 PgC $year^{-1}$). Our estimate of a total CO_2 removal by iron fertilisation within one century of 113 PgC is almost twice as high as the 60 PgC obtained with the PISCES model in a study that explicitly simulates the ecosystem response to iron fertilisation (Aumont and Bopp 2006). Other studies that assumed complete macro-nutrient draw-down in simpler biogeochemical models gave higher numbers by design (e.g. 120–277 PgC Jin and Gruber 2003, Cao and Caldeira 2010b). Zeebe and Archer (2005) estimate a lower reduction of 30 PgC as they consider only 15 fertilisation events per year South of 55°S. When fertilising only the Southern Ocean for 92 years about 60 PgC (or 0.6 PgC yr^{-1}) are taken up by the ocean in a study by Oschlies *et al* (2010a). The higher response in our model compared to Aumont and Bopp (2006) is partly due to larger areas of iron limitation in the Pacific Ocean in REcoM2 (figure 4). Models differ widely in the simulation of nutrient limitation in the Pacific (Laufkötter *et al* 2015), and recent evidence suggests that iron limitation could be more widespread than traditionally assumed based on macronutrient concentrations (Behrenfeld *et al* 2009, Nielsdóttir *et al* 2009). Aumont and Bopp (2006) use a lower limit for iron concentration of 0.01 nM to which iron is restored. In addition the models differ in the CO_2 scenarios (RCP8.5 in REcoM2, SRES98-A2 in PISCES) and whether they prescribe atmospheric CO_2 concentrations (REcoM2) or emissions (PISCES). The fact that REcoM2 prescribes concentrations and that we use a higher emission scenario can likely explain parts of the higher CO_2 removal potential. Furthermore, the ecosystem models differ in various details, e.g. variable C:N but fixed Fe:N ratios in the version of REcoM2 used here, compared to fixed C:N and variable C:Fe ratios in PISCES.

Our model simulates an export efficiency of 20% (export at 100 m relative to vertically integrated NPP) independent of Fe-availability. This is slightly higher than the 17% reported by Aumont and Bopp (2006), but lower than the 50% sequestration efficiency (at 1000 m) that Smetacek *et al* (2012) observed in an open ocean iron fertilisation experiment, in which the formation of fast sinking diatom aggregates accelerated carbon transport to the deep ocean.

The ratio of ΔCO_2 uptake to Δexport (relative to SI+ALK) decreases with time from approximately 85% at $\geqslant$1% Fe-availability (75% at 0.1% Fe-availability) to about 20% (12%) after 100 years (figure 5(b)) as expected due to remineralised carbon being transported back to the surface by the ocean circulation (Aumont and Bopp 2006). These numbers compare well with Aumont and Bopp (2006, 60% at start, 25% at end).

3.3. Feasibility and side-effects

Our study aims to estimate the carbon dioxide reduction potential (i.e. its upper limit) of the olivine dissolution approach by assuming total and instantaneous dissolution of the distributed olivine. Any real-world application of this approach might lead to a smaller molar ratio of oceanic CO_2 uptake per dissolved olivine simply due to an incomplete dissolution of the material within the surface mixed layer (Köhler *et al* 2013).

The iron contained in olivine increases the CDR potential of olivine dissolution by roughly 60% (figure 5(a) + (c)). At least 28% of the additional NPP and 40% of the increase in export production occurs in the Southern Ocean (table 2). The relative dissolution rate of olivine depends on temperature and on the depth of the mixed layer. Although the deep mixed layers in the Southern Ocean might lead to long residence time of distributed particles in the surface ocean, the low temperatures likely lead to slow dissolution rates (Köhler *et al* 2013), and a large fraction of the particles would probably sink undissolved to the abyss. Olivine dissolution rates were not yet derived for polar conditions (e.g. Hangx and Spiers 2009, Rimstidt *et al* 2012). Köhler *et al* (2013) estimate relative olivine dissolution rates around 50% between 40 and 60°S and between 10% and 40% south of 60°S. Olivine dissolution rates from long-term laboratory experiments are an order of magnitude smaller than from shorter experiments due to the growth of a biotic community at the surface of the rock (Oelkers *et al* 2015). Dissolution kinetics estimated in Köhler *et al* (2013) might therefore be faster than what might be achievable in nature. In addition, there are few ships going to the Southern Ocean (Köhler *et al* 2013). Therefore a distribution of olivine from ballast water of ships of opportunity is only possible north of 40°S. To gain the full CO_2 uptake potential calculated with our model,

about 300 large ships (net tonnage of 300 000 t each) would be needed with year-round commitment for an annual distribution of 3 Pg of olivine (Köhler *et al* 2013). Note that ice coverage and weather conditions will not allow transporting olivine to polar regions all year round.

Olivine dissolution leads to a maximum DIC increase of 40 mmol m^{-3} at 300–400 m depth. Assuming a typical C:-O_2 ratio of 117:170 (Anderson and Sarmiento 1994) gives an estimate of maximum oxygen consumption by iron fertilisation in the Southern Ocean of about 58 mmol m^{-3} (or 1.3 mL L^{-1}). This is on the order of <25% of the background oxygen concentration (Garcia *et al* 2014), but it could occur in addition to an oxygen reduction of up to 20 mmol m^{-3} in the mixed layer of the Southern Ocean as a response to climate change (Cocco *et al* 2013).

The radiative benefit of the iron and silicate fertilisation effects with olivine dissolution might be partly offset by N_2O production that accompanies organic matter remineralisation. This effect is smallest (compensates 13% of radiative benefit by iron fertilisation) in the Southern Ocean where 30% of the fertilisation occurs, but could amount up to 40% of the radiative benefit in the equatorial Pacific, the second largest region of iron fertilisation in our simulations (Jin and Gruber 2003).

Since olivine contains also a large fraction of other trace metals, such as nickel and chromium (De Hoog *et al* 2010), their input in the ocean and their potential harmful impact on marine ecosystems need to be assessed. Also note that undissolved particles in the surface ocean might reduce downwelling light intensities, and even modify ocean albedo. While the first of these side-effects has briefly been discussed in Köhler *et al* (2013), for the second a coupled atmosphere-ocean model would be needed. Further uncertainties arise from possible ecosystem shifts, shading of benthic ecosystems (Powell 2008) and phytoplankton-light-feedbacks that could lead to a warming of the sea surface (Manizza *et al* 2008) and a solubility-driven reduction of CO_2 uptake.

Geoengineering methods such as olivine dissolution are nowadays only investigated in model simulations. Any efforts to either test or implement ocean-based geoengineering approaches need to concur with existing international agreements such as the 'Convention on the Prevention of Marine Pollution by Dumping of Wastes and Other Matter', known as the London Convention (1972) and the later 1996 protocol, known as London Protocol (1996). The London Protocol has indeed extended its regularities on the issue of geoengineering on its 8th meeting in 2013 (reports can be found at https://webaccounts.imo.org) and any future ocean fertilisation experiments (performed by the contracting countries of the London Protocol) are regulated and need to fulfil the requirements of the protocol.

4. Summary and conclusions

Open ocean dissolution of olivine enhances marine CO_2 uptake by increasing the alkalinity concentration in the surface ocean and therefore the ocean's buffering capacity. In addition, marine primary and export production benefit from the fertilisation effects of silicic acid and iron. The relative contributions to total CO_2 uptake by olivine dissolution are 57% alkalinity, 37% iron and 6% silicic acid. The effects add up linearly with small synergistic effects. Alkalinity and silicic acid effects scale linearly with the amount of olivine, but the iron fertilisation runs into saturation, when the iron input reaches 2.3 Tg per year leading to a maximum iron-based carbon uptake rate of 113 PgC per century (or ~1.1 PgC per year on average, decreasing with time).

A global deployment of olivine to the open ocean can potentially sequester 0.57 PgC per Pg olivine in our model. Since we neglect the rebound effect by prescribing atmospheric CO_2 this value is likely lower in the real world. Furthermore, this theoretical value will likely never be reached (1) because real-world olivine dissolution is not instantaneous and total and especially slow in the Southern Ocean where at least 40% of the iron fertilisation effects occur, and (2) because of the poor accessibility of the Southern Ocean that is not regularly crossed by ships of opportunity.

On time scales of weeks to months, alkalinisation increases surface ocean pH, driving enhanced oceanic uptake of CO_2. However, after equilibration with the atmosphere, the addition of 3 Pg olivine yr^{-1} is not compensating the effect of ocean acidification and can lead to CO_2 uptake of no more than 1.7 PgC yr^{-1} which is small compared to the current anthropogenic CO_2 emissions (estimated to 9.9 PgC yr^{-1} for the year 2014, Le Quéré *et al* 2015).

To counteract acidification, open ocean dissolution of olivine can only be an additional measure to massive reductions in CO_2 emissions. The iron fertilisation reduces pH on the timescale of >50 years relative to an ocean alkalinisation experiment without iron due to the upwelling of remineralised carbon.

Acknowledgments

JH received funding from the Helmholtz PostDoc programme, CV from the German BMBF project SOPRAN.

References

Anderson L A and Sarmiento J L 1994 Redfield ratios of remineralisation determined by nutrient data analysis *Glob. Biogeochemical Cycles* **8** 65–80

Archer D 2005 Fate of fossil fuel CO_2 in geologic time *J. Geophys. Res.* **110** C09S05

Aumont O and Bopp L 2006 Globalizing results from ocean in situ iron fertilization studies *Glob. Biogeochem. Cycles* **20** GB2017

Baker A and Croot P 2010 Atmospheric and marine controls on aerosol iron solubility in seawater *Mar. Chem.* **120** 4–13
Behrenfeld M J and Milligan A J 2013 Photophysiological expressions of iron stress in phytoplankton *Annu. Rev. Mar. Sci.* **5** 217–46
Behrenfeld M J *et al* 2009 Satellite-detected fluorescence reveals global physiology of ocean phytoplankton *Biogeosciences* **6** 779–94
Cao L and Caldeira K 2010a Atmospheric carbon dioxide removal: long-term consequences and commitment *Environ. Res. Lett.* **5** 024011
Cao L and Caldeira K 2010b Can ocean iron fertilization mitigate ocean acidification? *Clim. Change* **99** 303–11
Cocco V *et al* 2013 Oxygen and indicators of stress for marine life in multi-model global warming projections *Biogeosciences* **10** 1849–68
De Baar H J, De Jong J T, Bakker D C, Löscher B M, Veth C, Bathmann U and Smetacek V 1995 Importance of iron for plankton blooms and carbon dioxide drawdown in the Southern Ocean *Nature* **373** 412–5
De Hoog J C, Gall L and Cornell D H 2010 Trace-element geochemistry of mantle olivine and application to mantle petrogenesis and geothermobarometry *Chem. Geol.* **270** 196–215
Egleston E S, Sabine C L and Morel F M M 2010 Revelle revisited: buffer factors that quantify the response of ocean chemistry to changes in DIC and alkalinity *Glob. Biogeochem. Cycles* **24** GB1002
Enting I, Wigley T and Heimann M 1994 Future emissions and concentrations of carbon dioxide: key ocean/atmosphere/land analyses *Technical Report* 31 CSIRO Division of Atmospheric Research, Melbourne
Fishwick M P, Sedwick P N, Lohan M C, Worsfold P J, Buck K N, Church T M and Ussher S J 2014 The impact of changing surface ocean conditions on the dissolution of aerosol iron *Glob. Biogeochemical Cycles* **28** 1235–50
Garcia H E, Locarnini R A, Boyer T P, Antonov J I, Baranova O K, Zweng M M, Reagan J and Johnson D R 2014 World ocean atlas 2013, volume 3: dissolved oxygen, apparent oxygen utilisation, and oxygen saturation *NOAA Atlas NESDIS 75* ed S Levitus and A Mishonov (Washington, DC: US Government Printing Office) p 27 (http://data.nodc.noaa.gov/woa/WOA13/DOC/woa13_vol3.pdf)
Geider R J, MacIntyre H L and Kana T M 1998 A dynamic regulatory model of phytoplankton acclimation to light, nutrients, and temperature *Limnology Oceanogr.* **43** 679–94
Glienke S, Irvine P J and Lawrence M G 2015 The impact of geoengineering on vegetation in experiment G1 of the geomip *J. Geophys. Res.* **120** 10, 196–10, 213
Hangx S J and Spiers C J 2009 Coastal spreading of olivine to control atmospheric CO_2 concentrations: a critical analysis of viability *Int. J. Greenhouse Gas Control* **3** 757–67
Hartmann J, West J, Renforth P, Köhler P, De La Rocha C, Wolf-Gladrow D, Dürr H and Scheffran J 2013 Enhanced chemical weathering as a geoengineering strategy to reduce atmospheric carbon dioxide, a nutrient source and to mitigate ocean acidification *Rev. Geophys.* **51** 113–49
Hauck J and Völker C 2015 Rising atmospheric CO_2 leads to large impact of biology on Southern Ocean CO_2 uptake via changes of the Revelle factor *Geophys. Res. Lett.* **42** 1459–64
Hauck J, Völker C, Wang T, Hoppema M, Losch M and Wolf-Gladrow D A 2013 Seasonally different carbon flux changes in the Southern Ocean in response to the Southern annular mode *Glob. Biogeochemical Cycles* **27** 1236–45
Honeyman B D and Santschi P H 1989 A Brownian-pumping model for oceanic trace metal scavenging: evidence from Th isotopes *J. Mar. Res.* **47** 951–92
International Energy Agency 2014 *World Energy Outlook* (Paris) (www.worldenergyoutlook.org)
IPCC 2013 Summary for policymakers *Climate Change 2013: The Physical Science Basis. Contribution of Working Group I to the Fifth Assessment Report of the Intergovernmental Panel on Climate Change* ed T Stocker *et al* (Cambridge: Cambridge University Press) (http://www.ipcc.ch/pdf/assessment-report/ar5/wg1/WG1AR5_SPM_FINAL.pdf)
Jin X and Gruber N 2003 Offsetting the radiative benefit of ocean iron fertilization by enhancing N_2O emissions *Geophys. Res. Lett.* **30** 2249
Jones A *et al* 2013 The impact of abrupt suspension of solar radiation management (termination effect) in experiment g2 of the geoengineering model intercomparison project (geomip) *J. Geophys. Res.* **118** 9743–52
Keeling R, Piper S, Bollenbacher A and Walker J 2009 Atmospheric CO_2 records from sites in the SIO air sampling network *Trends: A Compendium of Data on Global Change* Carbon Dioxide Information Analysis Center, Oak Ridge National Laboratory, US Department of Energy, Oak Ridge, Tenn., USA
Keller D P, Feng E Y and Oschlies A 2014 Potential climate engineering effectiveness and side effects during a high carbon dioxide-emission scenario *Nat. Commun.* **5** 3304
Köhler P, Abrams J F, Völker C, Hauck J and Wolf-Gladrow D A 2013 Geoengineering impact of open ocean dissolution of olivine on atmospheric CO_2, surface ocean pH and marine biology *Environ. Res. Lett.* **8** 014009
Köhler P, Hartmann J and Wolf-Gladrow D A 2010 Geoengineering potential of artificially enhanced silicate weathering of olivine *Proc. Natl Acad. Sci.* **107** 20228–33
Kravitz B, Robock A, Boucher O, Schmidt H, Taylor K E, Stenchikov G and Schulz M 2011 The geoengineering model intercomparison project (GeoMIP) *Atmos. Sci. Lett.* **12** 162–7
Kravitz B *et al* 2013 Climate model response from the geoengineering model intercomparison project (GeoMIP) *J. Geophys. Res.* **118** 8320–32
Large W and Yeager S 2009 The global climatology of an interannually varying air–sea flux data set *Clim. Dyn.* **33** 341–64
Laufkötter C *et al* 2015 Drivers and uncertainties of future global marine primary production in marine ecosystem models *Biogeosciences* **12** 6955–84
Le Quéré C *et al* 2015 Global carbon budget 2014 *Earth Syst. Sci. Data* **7** 47–85
Liu X and Millero F J 2002 The solubility of iron in seawater *Mar. Chem.* **77** 43–54
London Convention 1972 Convention on the prevention of marine pollution by dumping of wastes and other matter (http://imo.org/OurWork/Environment/LCLP/Documents/LC1972.pdf)
London Protocol 1996 Protocol to the 1972 convention on the prevention of marine pollution by dumping of wastes and other matter (http://imo.org/OurWork/Environment/LCLP/Documents/PROTOCOLAmended2006.pdf)
Mahowald N M, Baker A R, Bergametti G, Brooks N, Duce R A, Jickells T D, Kubilay N, Prospero J M and Tegen I 2005 Atmospheric global dust cycle and iron inputs to the ocean *Glob. Biogeochem. Cycles* **19** GB4025
Manizza M, Le Quéré C, Watson A J and Buitenhuis E T 2008 Ocean biogeochemical response to phytoplankton-light feedback in a global model *J. Geophys. Res.* **113** C10010
Marshall J, Adcroft A, Hill C, Perelman L and Heisey C 1997 A finite-volume, incompressible Navier Stokes model for studies of the ocean on parallel computers *J. Geophys. Res.* **102** 5753–66
Martin J H and Fitzwater S E 1988 Iron deficiency limits phytoplankton growth in the north–east Pacific subarctic *Nature* **331** 341–3
Matthews H D 2010 Can carbon cycle geoengineering be a useful complement to ambitious climate mitigation? *Carbon Manage.* **1** 135–44
Meinshausen M *et al* 2011 The RCP greenhouse gas concentrations and their extensions from 1765 to 2300 *Clim. Change* **109** 213–41
MITgcm Group 2015 MITgcm user manual (online documentation) MIT/EAPS, Cambridge, MA, USA

(http://mitgcm.org/public/r2 manual/latest/online documents/manual.pdf)
National Research Council 2015 *Climate Intervention: Reflecting Sunlight to Cool Earth* (Washington, DC: The National Academies) (http://www.nap.edu/catalog/18988/climate-interventionreflecting-sunlight-to-cool-earth)
Nielsdóttir M C, Moore C M, Sanders R, Hinz D J and Achterberg E P 2009 Iron limitation of the postbloom phytoplankton communities in the Iceland Basin *Glob. Biogeochem. Cycles* **23** GB3001
Oelkers E H, Benning L G, Lutz S, Mavromatis V, Pearce C R and Plümper O 2015 The efficient long-term inhibition of forsterite dissolution by common soil bacteria and fungi at Earth surface conditions *Geochim. Cosmochim. Acta* **168** 222–35
Oschlies A 2009 Impact of atmospheric and terrestrial CO_2 feedbacks on fertilization-induced marine carbon uptake *Biogeosciences* **6** 1603–13
Oschlies A, Koeve W, Rickels W and Rehdanz K 2010a Side effects and accounting aspects of hypothetical large-scale Southern Ocean iron fertilization *Biogeosciences* **7** 4017–35
Oschlies A, Pahlow M, Yool A and Matear R J 2010b Climate engineering by artificial ocean upwelling: channelling the sorcerer's apprentice *Geophys. Res. Lett.* **37** L04, 701
Pörtner H-O, Karl D, Boyd P, Cheung W, Lluch-Cota S, Nojiri Y, Schmidt D and Zavialov P 2014 Ocean systems *Climate Change 2014: Impacts, Adaptation, and Vulnerability. Part A: Global and Sectoral Aspects. Contribution of Working Group II to the Fifth Assessment Report of the Intergovernmental Panel on Climate Change* ed C Field *et al* (Cambridge: Cambridge University Press) pp 411–484
Powell H 2008 What are the possible side effects? The uncertainties and unintended consequences of manipulating ecosystems *Oceanus Mag.* **46** 14–7
Raven J A 1988 The iron and molybdenum use efficiencies of plant growth with different energy, carbon and nitrogen sources *New Phytologist* **109** 279–87
Rimstidt J D, Brantley S L and Olsen A A 2012 Systematic review of forsterite dissolution rate data *Geochim. Cosmochim. Acta* **99** 159–78
Rodgers K B, Blanke B, Madec G, Aumont O, Ciais P and Dutay J-C 2003 Extratropical sources of equatorial pacific upwelling in an ogcm *Geophys. Res. Lett.* **30** 1084
Rogelj J, Schaeffer M, Meinshausen M, Knutti R, Alcamo J, Riahi K and Hare W 2015 Zero emission targets as long-term global goals for climate protection *Environ. Res. Lett.* **10** 105007
Rose A L and Waite T D 2007 Reconciling kinetic and equilibrium observations of iron(III) solubility in aqueous solutions with a polymer-based model *Geochim. Cosmochim. Acta* **71** 5605–19
Sarmiento J, Gruber N, Brzezinski M and Dunne J 2004 High-latitude controls of thermocline nutrients and low latitude biological productivity *Nature* **427** 56–60
Schuiling R and Krijgsman P 2006 Enhanced weathering: an effective and cheap tool to sequester CO_2 *Clim. Change* **74** 349–54
Smetacek V *et al* 2012 Deep carbon export from a Southern Ocean iron-fertilized diatom bloom *Nature* **487** 313–9
UNFCCC 2009 Copenhagen accord (http://unfccc.int/resource/docs/2009/cop15/eng/l07.pdf)
van Vuuren D *et al* 2011 The representative concentration pathways: an overview *Clim. Change* **109** 5–31
Zeebe R and Archer D 2005 Feasibility of ocean fertilization and its impact on future atmospheric CO_2 levels *Geophys. Res. Lett.* **32** L09703

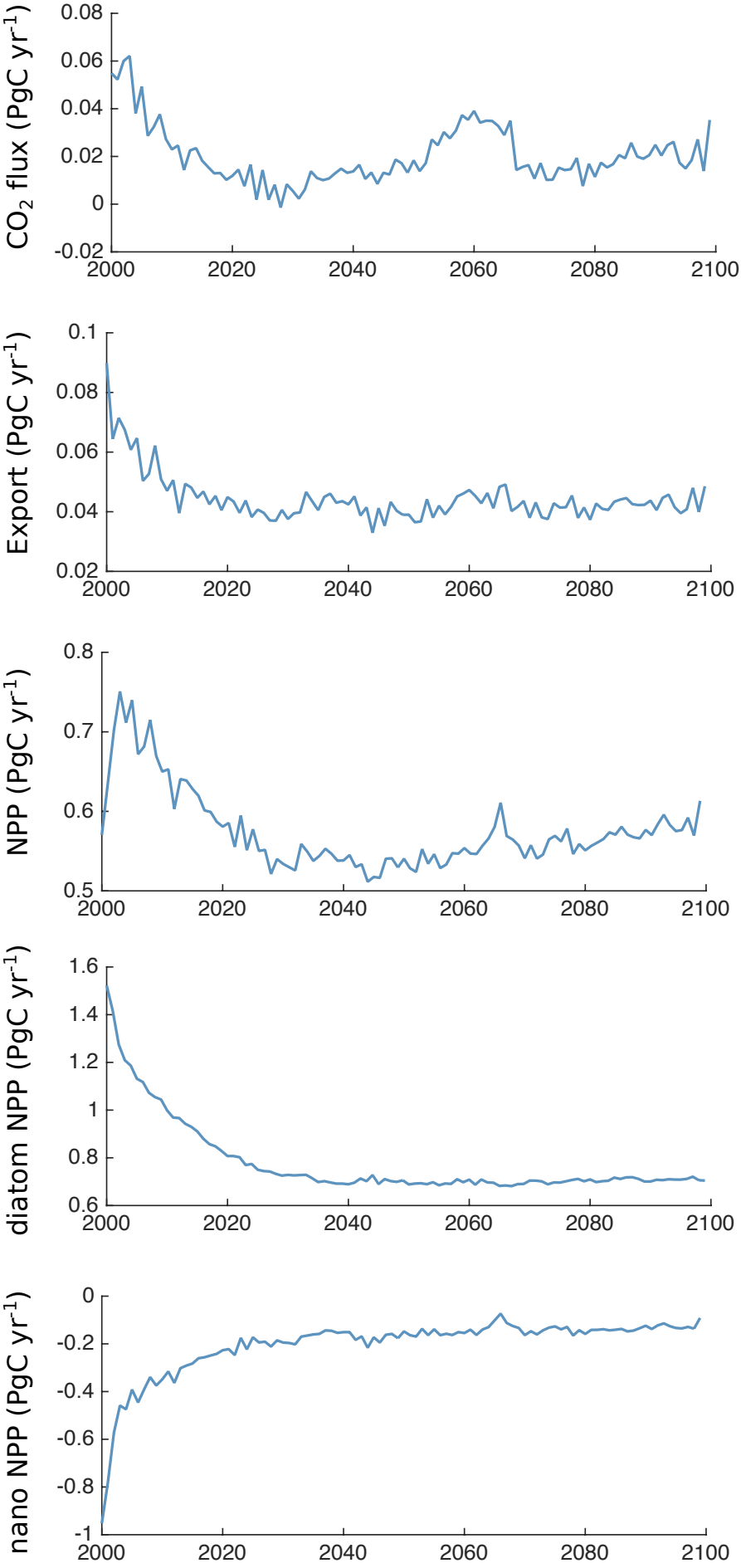

Figure S1: Synergistic effects of silicic acid and iron addition on primary and export production and CO_2 flux.

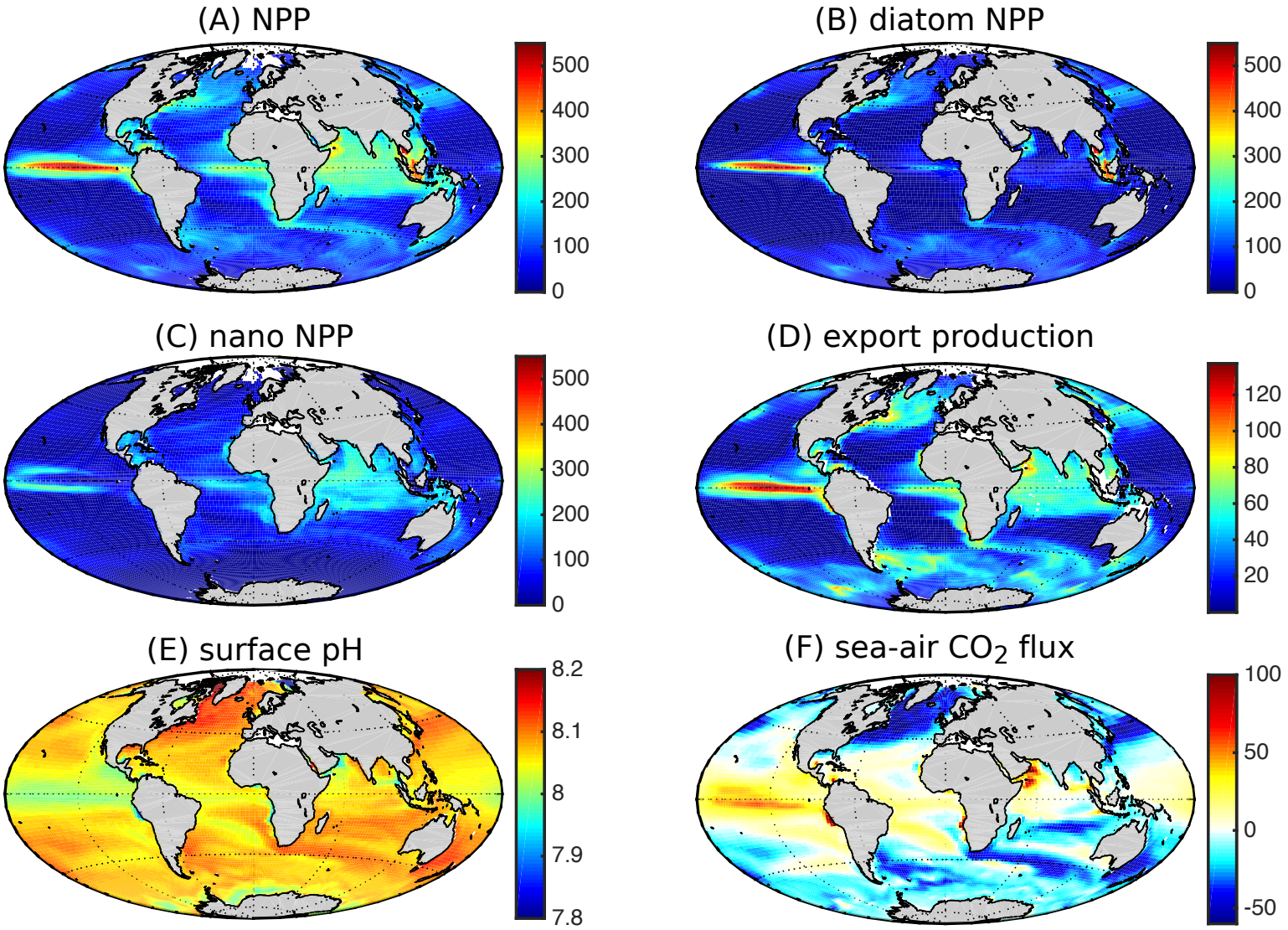

Figure S2: Mean fields in the first 10 years (2000-2009) of the control (CTRL) run. Shown are (A) vertically-integrated total net primary production (NPP), (B) diatom NPP, (C) nanophytoplankton NPP, (D) export production at 100 m, (E) surface pH and (F) CO_2 flux (negative: into the ocean). All units in gC m^{-2} yr^{-1}, except pH, which is unitless.

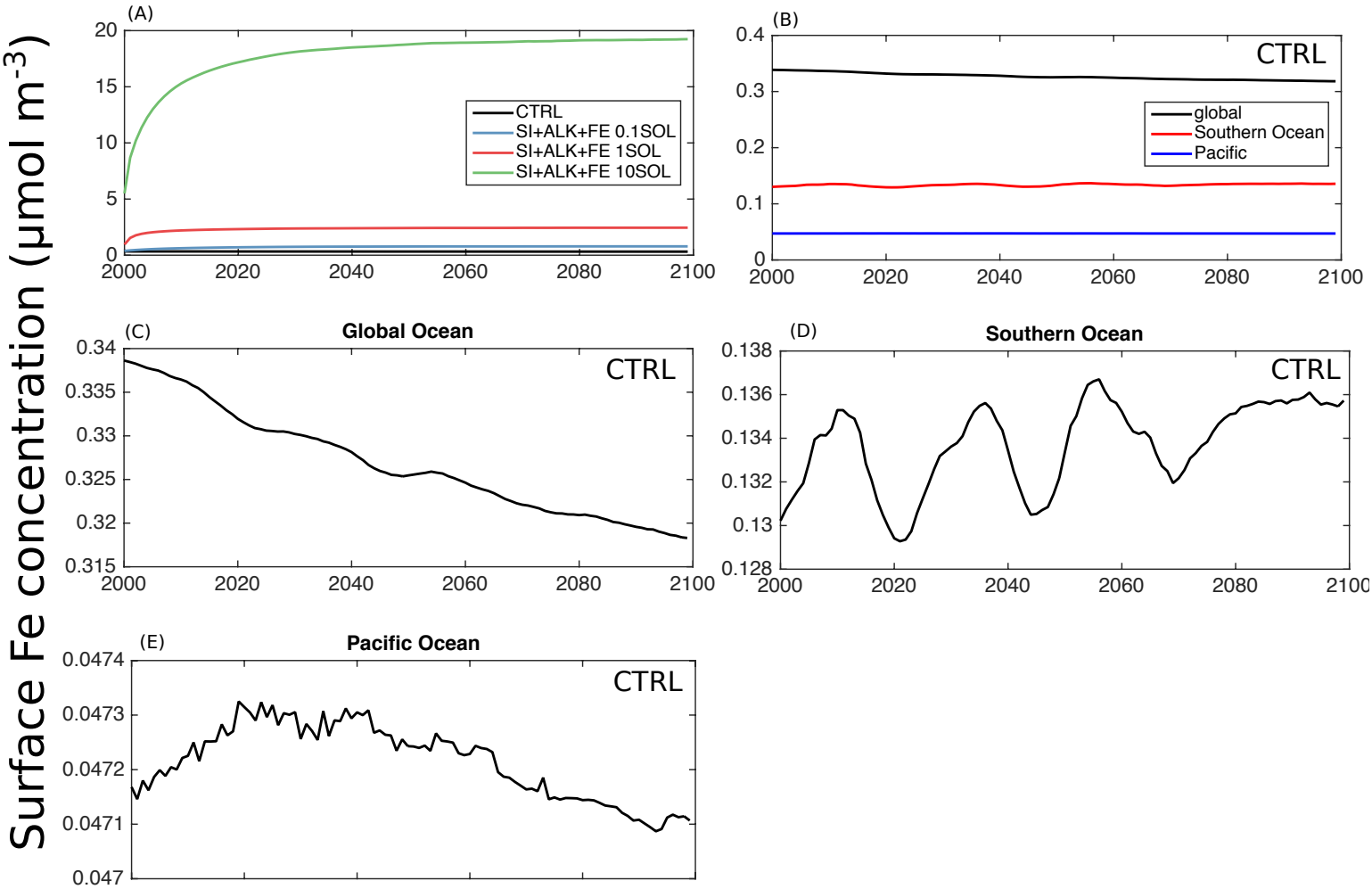

Figure S3:Time-series of surface iron concentration (μmol m^{-3}) for (A) the global ocean in the CTRL simulation and olivine dissolution scenarios, for (B) the CTRL simulation in the global, Southern and Pacific Oceans and (C-E) a close-up of the time-series in the global, Southern and Pacific Oceans. Note the different scales in all panels. The Southern Ocean is defined as south of 40°S, and the Pacific Ocean is between 30°S to 60°N and between 130°E to 110°W.